JOURNAL OF GEOPHYSICAL RESEARCH, VOL. 115, D01204, doi:10.1029/2009JD012487, 2010

Seasonal characteristics of aerosol radiative effect estimated from ground-based solar radiation measurements in Tsukuba, Japan

Rei Kudo,[1] Akihiro Uchiyama,[1] Akihiro Yamazaki,[1] and Eriko Kobayashi[2]

Received 15 May 2009; revised 7 October 2009; accepted 16 October 2009; published 15 January 2010.

[1] The seasonal characteristics of aerosol optical properties and surface direct radiative forcing were evaluated from ground-based solar radiation measurements under cloudless conditions in Tsukuba, Japan, from April 2004 to March 2008. Optical thickness (τ), single scattering albedo (ω_0), and asymmetry factor (g) at visible and near-infrared wavelengths were estimated from the direct and diffuse spectral irradiances. The radiative forcings in total, visible, and near-infrared regions were estimated from the measured direct and diffuse broadband irradiances. The value of τ was large from spring to summer and small in winter; ω_0 was large in summer and small in winter; and g was large in spring and small in summer, but there is a possibility of underestimating g due to the uncertainty in the estimated size distribution. The radiative forcing (AF^{24}) had almost the same seasonal changes as those of τ. However, the radiative forcing efficiency (AFE^{24}), defined as AF^{24} per unit τ, was not consistent with ω_0 and g. The fractional radiative focing efficiency ($FAFE^{24}$) was defined as a ratio of AFE^{24} to the solar irradiance at the top of the atmosphere, and a close correlation was found among ω_0, g, and $FAFE^{24}$. The seasonal radiative effects of aerosols were clarified by $FAFE^{24}$. These evaluated τ, ω_0, g, and AF^{24} were compared with those at other sites over East Asia. The values of τ, ω_0, g, and AF^{24} in Japan were smaller than those over the continent at all seasons. These differences suggest that the aerosols in Japan have different compositions from those over the continent.

Citation: Kudo, R., A. Uchiyama, A. Yamazaki, and E. Kobayashi (2010), Seasonal characteristics of aerosol radiative effect estimated from ground-based solar radiation measurements in Tsukuba, Japan, *J. Geophys. Res.*, *115*, D01204, doi:10.1029/2009JD012487.

1. Introduction

[2] Aerosols affect the radiative budget of the Earth atmosphere system directly by scattering and absorbing solar radiation and indirectly by influencing cloud properties and lifetimes [*Charlson et al.*, 1992]. In this study, we concentrate on the aerosol direct radiative forcing at the Earth's surface, which is usually defined as the difference between the surface solar irradiances with and without aerosols. To understand the aerosol surface radiative forcing, three optical properties in the total atmospheric column are necessary: optical thickness (loading), single-scattering albedo (ratio of scattering to scattering + absorption), and asymmetry factor (asymmetry of forward and backward scattering).

[3] Aerosol lifetimes are only a week or less, and there are substantial uncertainties in their spatial and temporal variations. Ground-based remote sensing does not provide global coverage. However, its spectral measurements of solar and sky radiation continuously provide the reliable optical properties and are suitable for evaluating the aerosol radiative effects in the long term. In recent years, ground-based aerosol/radiation observation networks such as Sky-radiometer Network (SKYNET) (http://atmos.cr.chiba-u.ac.jp/aerosol/skynet) and Aerosol Robotic Network (AERONET) [*Holben et al.*, 1998] have been deployed over East Asia, which is well recognized as a major source of natural and anthropogenic aerosols. Their observations indicated that the aerosol optical properties in the Asian continent have greater optical thickness and lower single-scattering albedo than those of the same type of aerosols found in other areas [e.g., *Kim et al.*, 2004, 2005; *Cheng et al.*, 2006]. These aerosols in the Asian continent are transported to the North Pacific Ocean via Japan by the westerlies in the midlatitudes. *Kaneyasu et al.* [2000] demonstrated that the cold outflow from the Asian continent in winter has a high mass ratio of black carbon (BC). *Uchiyama et al.* [2005a, 2005b] found that coarser dust particles from the Asian continent during the spring dust event are partially removed and that the single-scattering albedo becomes lower during transportation to Japan. *Pradeep and Ishizaka* [2007] found that optical thickness and single-scattering albedo of aerosols from the Asian continent are modified by relative humidity and mixing of components over the East China Sea. These studies suggest that the transported continental aerosols

[1] Meteorological Research Institute, Japan Meteorological Agency, Tsukuba, Japan.
[2] Aerological Observatory, Japan Meteorological Research Agency, Tsukuba, Japan.

0148-0227/10/2009JD012487$09.00

differ by season and are modified under different atmospheric conditions during the transportation. Japan is located off the eastern edge of the Asian continent. The atmosphere over Japan is affected by the continental aerosols, but the aerosol optical properties observed over Japan have different features from the continental aerosols. However, there are not many studies regarding the seasonal characteristics of the aerosol optical properties and radiative forcing in Japan.

[4] In order to assess the aerosol effects on the radiative budget of the atmosphere, we have conducted the spectral and broadband measurements of the surface solar radiation at the Meteorological Research Institute in Tsukuba, Japan, since 2004. In this study, we evaluate the seasonal changes of the aerosol optical properties and surface net radiative forcing on the basis of the measurements under cloudless conditions from April 2004 to March 2008. Optical thickness, single-scattering albedo, and asymmetry factor at visible and near-infrared (NIR) wavelengths are estimated from the measured direct and diffuse spectral irradiances. The surface net radiative forcing in the total (TTL), visible (VIS), and NIR regions is estimated from the measurements and calculations without aerosols of the direct and diffuse broadband irradiances. Furthermore, we investigate the seasonal relationship between the optical properties and surface net radiative forcing. In the last, we discuss the difference between this study and the results at other sites over East Asia.

2. Observations and Methods

2.1. Observations

[5] Our observatory is the Meteorological Research Institute (36.05°N, 140.13°E, about 25 m above sea level) in Tsukuba, Japan, about 50 km northeast of Tokyo. We have observed the surface solar radiation by two grating-type spectral radiometers and four broadband radiometers from April 2004 to March 2008. The direct and diffuse spectral irradiances were measured by a grating-type spectral pyrheliometer and a grating-type spectral pyranometer with a shadowing cube. These instruments were made by Prede Co. Ltd. The spectral pyrheliometer observes the direct irradiances at 350–1050 nm with 3.6 nm resolution. To avoid the strong gas-absorption wavelengths, 380, 400, 500, 675, 870, and 1020 nm are used to estimate the aerosol optical properties and 940 nm is used to estimate the precipitable water vapor. The calibration constants of each wavelength were determined by side-by-side comparison with our reference grating-type spectral pyrheliometer, which uses a spectroradiometer (Spectra Vista Corporation, GER 2600) and is calibrated by the Langley method from observations at the Mauna Loa Observatory every year. The grating-type spectral pyranometer with a shadowing cube observes the diffuse irradiances at 350–1050 nm with 3.6 nm resolution. Since the sensitivity at 1020 nm is too low to measure the diffuse irradiance under cloudless condition, the measurements at 380, 400, 500, 675, and 870 nm are used. The calibration constants of each wavelength were also determined by side-by-side comparison with our reference spectral pyrheliometer. In the comparison, a collimation tube was installed to measure the direct irradiance at the top of the spectral pyranometer. The cosine response of the spectral pyranometer was measured by irradiating a parallel beam of light onto the spectral pyranometer in the Japan Meteorological Agency (JMA) Meteorological Instrument Calibration Center in Tsukuba. The overall accuracies of measurements were less than 5% for direct irradiances, less than 6% for diffuse irradiances, and less than 0.02 for optical thickness. These accuracies were determined from calibration constants and cosine response errors.

[6] The direct and diffuse broadband irradiances in TTL and NIR were measured by two broadband pyrheliometers (Kipp and Zonen CH1) and two broadband pyranometers (Kipp and Zonen CM21) with shadowing cubes. The irradiances in TTL and NIR were measured with transparent (Schott WG305, 305–2900 nm) and red (Schott RG715, 715–2900 nm) filters, respectively. The irradiances in VIS were calculated as the difference between TTL and NIR. The global irradiances were calculated as the sum of the direct and diffuse irradiances to reduce the cosine response errors of the broadband pyranometers. The calibration constants of two broadband pyranometers and two broadband pyrheliometers were determined by side-by-side comparison with our reference broadband pyranometer (Kipp and Zonen CM22) and broadband pyrheliometer (Kipp and Zonen CH1). The reference instruments are regularly calibrated in the JMA Meteorological Instrument Calibration Center. *Nishizawa et al.* [2004] used the same broadband pyranometers as used in this study. They estimated that the overall relative accuracy of the instruments is within 2%. The pyrheliometers must be better because they do not have the cosine response.

2.2. Cloud Screening

[7] Considering only the radiative effect of aerosols on the solar radiation, the measurements under cloudy conditions were removed by the normalized clearness index of *Perez et al.* [1990]. The index is defined as

$$k_t = \frac{BF_{obs}(TTL)/S(TTL)}{1.031\exp\left(\frac{-1.4}{0.9+9.4/m_a}\right)+0.1}, \quad (1)$$

where $BF_{obs}(TTL)$ is the measured instantaneous global irradiance in TTL, $S(TTL)$ is the instantaneous solar irradiance in TTL at the top of the atmosphere, and m_a is optical air mass by *Kasten and Young* [1989]. The cloudless condition is defined as $k_t > 0.7$ by *Molineaux et al.* [1995]. However, *López and Batlles* [2004] pointed out that this criterion does not detect thin cloud cover as from cirrus clouds. Therefore, we detected the cloudless conditions by the following empirical criteria: (1) $k_t > 0.7$ and (2) $AVE(k_t) > 0.7$ and $STD(k_t) < 0.1$. $AVE(k_t)$ and $STD(k_t)$ are the average and the standard deviation of k_t over 10 minutes. The threshold of $STD(k_t)$ was determined empirically. We applied these criteria to several days in each season and checked the results by the pictures of the sky view camera. Figure 1 presents an example of the cloud screening.

2.3. Aerosol Optical Properties

[8] We have developed a method to estimate single-scattering albedo $\omega_0(\lambda_N)$ (λ_N = 380, 400, 500, 675, 870 nm) and asymmetry factor $g(\lambda_N)$ from the direct and diffuse spectral irradiances [*Kudo et al.*, 2008]. Here we used the

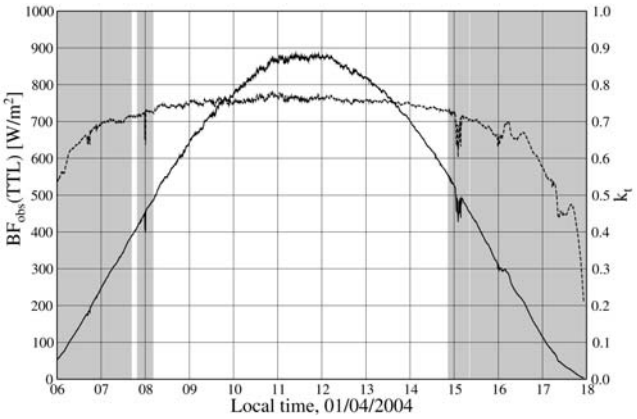

Figure 1. Example of cloud screening. Measured instantaneous global irradiance in TTL (solid line) and clearness index (broken line). The shaded area indicates cloudy conditions.

indirect method in the literature. The indirect method is based on the method of maximum likelihood and optimizes the refractive index (both imaginary and real parts) and the size distribution to the measured diffuse/direct ratio and optical thickness $\tau(\lambda_N)$. The optimization is conducted by the Newton-Gauss method. Variables $\omega_0(\lambda_N)$ and $g(\lambda_N)$ are calculated from the optimized refractive index and size distribution by Mie theory.

[9] The Newton-Gauss method is an iterative procedure and requires the initial parameters and the convergence criterion. We gave 1.5 – 0.005i as the initial refractive index and the Junge distribution as the initial size distribution. The Junge distribution consists of a scaling factor proportional to the aerosol concentration and a shaping constant. Two factors were determined from the observed optical thickness. The convergence criterion is that the optical thickness, direct spectral irradiances, and diffuse spectral irradiances calculated from the estimated refractive index and size distribution are within "measured values $\pm 1.96\sigma$" (σ is the measurement accuracy). This means that the estimated values are within the 95% confidence interval of a Gaussian distribution.

[10] The accuracies of estimated $\omega_0(\lambda_N)$ and $g(\lambda_N)$ are determined by the tests for the various aerosol types [*Kudo et al.*, 2008]. The accuracies are less than 0.03 for $\omega_0(\lambda_N)$ and less than 0.06 for $g(\lambda_N)$. The indirect method cannot retrieve the size distribution at radius >1.0 μm. In the case of dust type, $g(\lambda_N)$ is underestimated by the error of the size distribution. According to *Kudo et al.* [2008], the bias error is about 0.06. The error of the size distribution does not affect the retrieval of $\omega_0(\lambda_N)$. In order to fit the estimated diffuse/direct ratios to the measured ones, the indirect method overestimates the imaginary part of the refractive index. Therefore, $g(\lambda_N)$ is underestimated but $\omega_0(\lambda_N)$ is estimated well.

2.4. Daily Mean of the Aerosol Surface Net Radiative Forcing

[11] The surface net radiative forcing is usually defined as the difference between the global irradiances with and without aerosols. The first term is directly measured by the broadband radiometers, and the second term is calculated by the radiative transfer model. Since the instantaneous effects of aerosols on the surface irradiance heavily depend on the solar zenith angle, the daily means are better to represent the climate effects of aerosols. The daily mean of the net radiative forcing is estimated by the following procedures:

[12] 1. Selection of the measured instantaneous global irradiances $BF_{obs}(\lambda_B)$ (λ_B = *TTL*, *VIS*, *NIR*) under cloudless conditions in a day. The cloudless conditions were detected by the cloud screening method described in section 2.2. We analyzed the days in which total time under cloudless conditions exceeded 2 h in a day.

[13] 2. Calculation of the instantaneous global irradiances without aerosols $BF_{mol}(\lambda_B)$. $BF_{mol}(\lambda_B)$ were calculated by the radiative transfer model developed by *Asano and Shiobara* [1989] and *Nishizawa et al.* [2004]. The model atmosphere was assumed to be plane-parallel and was divided into 23 layers from the surface up to an altitude of 50 km. The solar spectrum between 300 and 2900 nm was divided into 50 intervals, and the irradiances were calculated by the doubling and adding method [*Lacis and Hansen*, 1974]. The gaseous absorptions by water vapor, carbon dioxide, oxygen, and ozone were included. The atmospheric vertical profiles of pressure and temperature were given from radiosonde measurements launched from Tateno Aerological Observatory (AO), located next to MRI. The concentration of carbon dioxide was given from the monthly means measured at Ryori (39.02°N, 141.49°E), one of the sites whose data are reported to the World Data Center for Greenhouse Gases. Total ozone was given from the monthly means measured at Tateno AO, one of the sites whose data are reported to the World Ozone and Ultraviolet Radiation Data Center. The precipitable water vapor was estimated by an empirical fitting between water transmittance at 940 nm measured by our spectral pyrheliometer and precipitable water vapor obtained from the radiosonde measurement at 0000 UTC. We employed the following relation of *Schmid et al.* [1996]:

$$T_W = \exp\left[-a(m_a u)^b\right], \tag{2}$$

where T_W is the water vapor transmittance at 940 nm, u is the precipitable water vapor from the radiosonde measurements, and $m_a u$ is the slant path water vapor amount. Figure 2 presents the results for all seasons. We determined a and b for spring, summer, autumn, and winter.

[14] 3. The daily means of $BF_{obs}(\lambda_B)$ and $BF_{mol}(\lambda_B)$ calculated by the empirical fitting. The primary factor that determines the magnitude of the diurnal cycle of $BF_{obs}(\lambda_B)$ under cloudless conditions is the solar zenith angle θ, and it is customary to empirically fit $BF_{obs}(\lambda_B)$ using the cosine of θ as the independent variable [*Long and Ackerman*, 2000]. *Waliser et al.* [1996] and *Chou and Zhao* [1997] estimated the daily means by polynomial functions, and *Long and Ackerman* [2000] used a power law function. We tested some fittings and selected the following second-order polynomial function as the simplest and stablest fitting:

$$BF^{fit}_{obs,mol}(\lambda_B, \theta) = a(\cos\theta)^2 + b(\cos\theta), \tag{3}$$

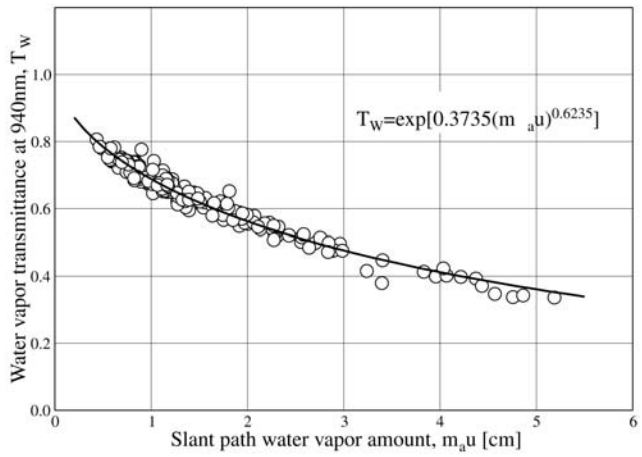

Figure 2. Water vapor transmittance at 940 nm measured by the spectral pyrheliometer versus slant path water vapor amount measured by radiosonde.

where $BF^{fit}_{obs,mol}$ (λ_B, θ) is the fitted instantaneous global irradiance and is assumed to be zero at $\theta = 90°$. Figure 3 is an example of fitting.

[15] 4. Calculation of the daily mean of the surface net radiative forcing AF^{24} (λ_B). Using equation (3), AF^{24} (λ_B) is calculated by

$$BF^{24}_{obs}(\lambda_B) = \int_{24h} BF^{fit}_{obs}(\lambda_B, \theta)dt/24h, \quad (4)$$

$$BF^{24}_{mol}(\lambda_B) = \int_{24h} BF^{fit}_{mol}(\lambda_B, \theta)dt/24h, \quad (5)$$

$$AF^{24}(\lambda_B) = (1 - Rs(\lambda_B))\left(BF^{24}_{obs}(\lambda_B) - BF^{24}_{mol}(\lambda_B)\right), . \quad (6)$$

where $R_S(\lambda_B)$ is the surface albedo and is 0.14 for TTL, 0.09 for VIS, and 0.19 for NIR. These values were estimated from the upward and downward solar irradiance measurements by radiometersondes [*Asano et al.*, 1997].

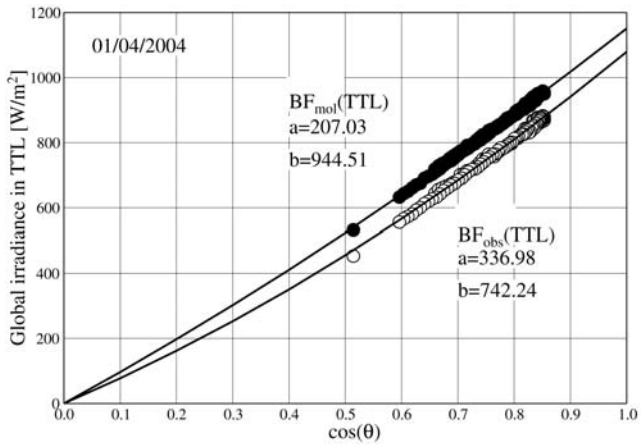

Figure 3. Example of second-order polynomial fitting to measured global irradiance (open circle) and global irradiance calculated without aerosols (filled circle).

[16] In this study, the aerosol optical properties and surface net radiative forcing are estimated from different instruments. In order to discuss the relations between the optical properties and surface net radiative forcing, we must ensure that the measured global irradiances agree with the global irradiances calculated from the estimated optical properties. However, estimated τ is limited to 380–1020 nm, and ω_0 and g are limited to 380–870 nm. Therefore, we used a linear regression method on log λ – log τ, ω_0, g plane [*Won et al.*, 2004]. In calculating the global irradiances, the aerosol phase function was determined from g by the modified Hennyey-Greenstein phase function [*Cornette and Shanks*, 1992]. Figure 4 presents the results of the comparisons of all the data in this study. The calculated global irradiance in VIS was underestimated by about 4% with a root mean square error (RMSE) of 16 W/m^2. The agreement is good, considering the assumed phase function and measurement accuracy. The calculated global irradiance in NIR was overestimated by 19% with an RMSE of 69 W/m^2. The reason for the large error is that most of the optical properties in NIR are extrapolated. The calculated global irradiance in TTL was overestimated by 7% with an RMSE of 59 W/m^2. This error is almost the same as in the other studies [*Won et al.*, 2004; *Kim et al.*, 2005].

2.5. Aerosol Surface Net Radiative Forcing Efficiency

[17] In general, AF^{24} has an almost linear dependence on τ. The surface net radiative forcing efficiency AFE^{24} is defined as AF^{24} per unit τ. AFE^{24} depends primarily on ω_0 and secondarily on g, according to some studies [e.g., *Nakajima et al.*, 2003; *Kim et al.*, 2005]. AFE^{24} is very useful for discussing the relationship between AF^{24} and optical properties. In this study, AFE^{24} is calculated from a linear regression as $AF^{24} = AFE^{24}\ \tau$. Variable τ(500) is used for AFE^{24} (*TTL*) and AFE^{24} (*VIS*). Variable τ(870) is used for

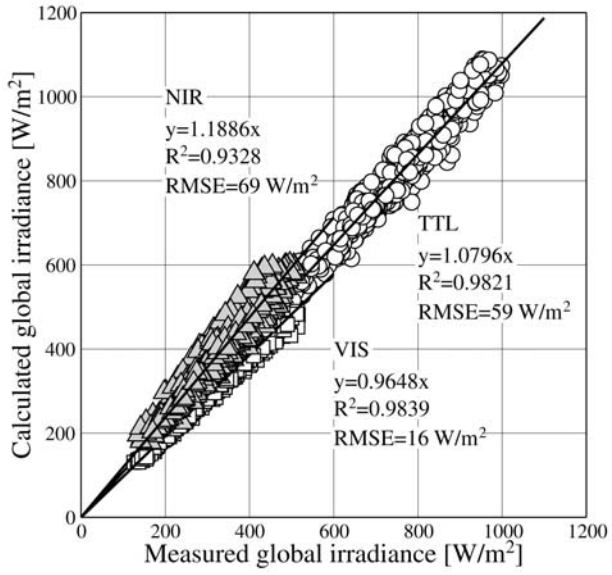

Figure 4. Comparison between measured and calculated global irradiances for TTL (open circles), VIS (squares), and NIR (shaded triangles). "R^2" and "RMSE" denote the coefficient of determination and root mean square error.

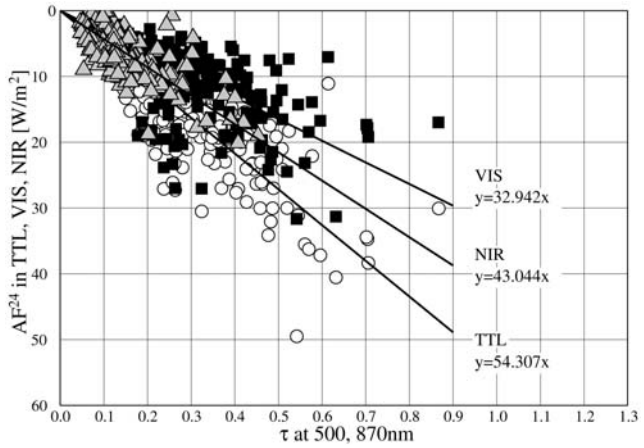

Figure 5. Aerosol surface net radiative forcing efficiency for TTL (open circles), VIS (filled squares), and NIR (shaded triangles).

AFE^{24} (*NIR*). Figure 5 presents the results for all seasons. The monthly AFE^{24} is presented in section 3.

3. Results and Discussions

3.1. Sampling Number

[18] Figure 6 shows the number of the analyzed days in each month. The total number is 211 days in 4 years: 88 days in spring (March–May), 14 days in summer (June–August), 20 days in autumn (September–November), and 89 days in winter (December–February). In Tsukuba, summer and autumn are wet seasons, and spring and winter are dry seasons. Therefore, there are few analyzed days in summer and autumn.

3.2. Aerosol Optical Properties

[19] Figure 7 depicts the monthly means of τ and Ångström exponent α. In this study, we used 500 nm as a representative wavelength of TTL and VIS and 870 nm as a representative wavelength of NIR. Variable τ(500) was from 0.15 to 0.39, large from spring to summer and small in winter. Variable τ(870) was from 0.07 to 0.19, large from spring to summer and small in winter. Variable α was from 1.1 to 1.8, small in the dry season (winter and spring) and large in the wet season (summer and autumn). The seasonal change of α indicates that the coarse particles are more dominant in the dry season than in the wet season. Figure 8 presents the monthly means of the volume size distribution. Notice that the size distribution at radius >1 μm cannot be estimated by our retrieval method. In the dry season, the coarse particles are dominant because they are emitted from the dry soil. Furthermore, dust coming from the Asian continent is a cause of large τ in spring. By contrast, there are few coarse particles emitted from the soil in the wet season because rainy conditions continue and the soil is wet and covered with grass. Additionally, the strong sunshine and wet conditions accelerate the generation of small particles because of the gas-to-particle conversion process. Therefore, the small particles become dominant in the wet season. Furthermore, *Hayasaka et al.* [1998] and *Nishizawa et al.* [2004] pointed out that the weak southern wind is dominant in summer and the hazy air is transported from Tokyo, causing a large τ.

[20] Figure 7 also presents the monthly means of ω_0. Variable ω_0(500) was from 0.67 to 0.86, large in summer and small in winter. This is almost the same as the work of *Nishizawa et al.* [2004], from 0.69 to 0.87. Variable ω_0(870)

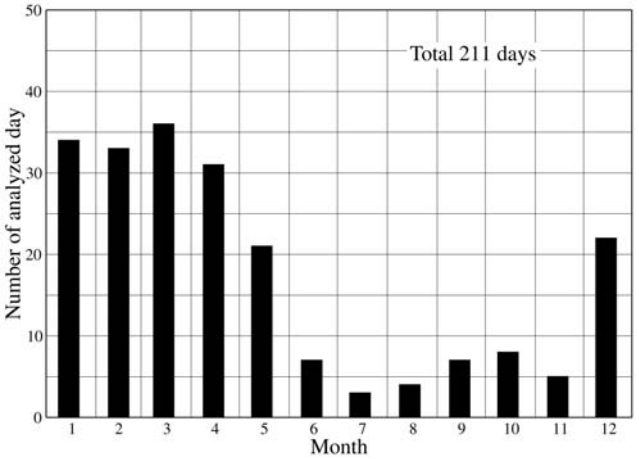

Figure 6. Number of analyzed days.

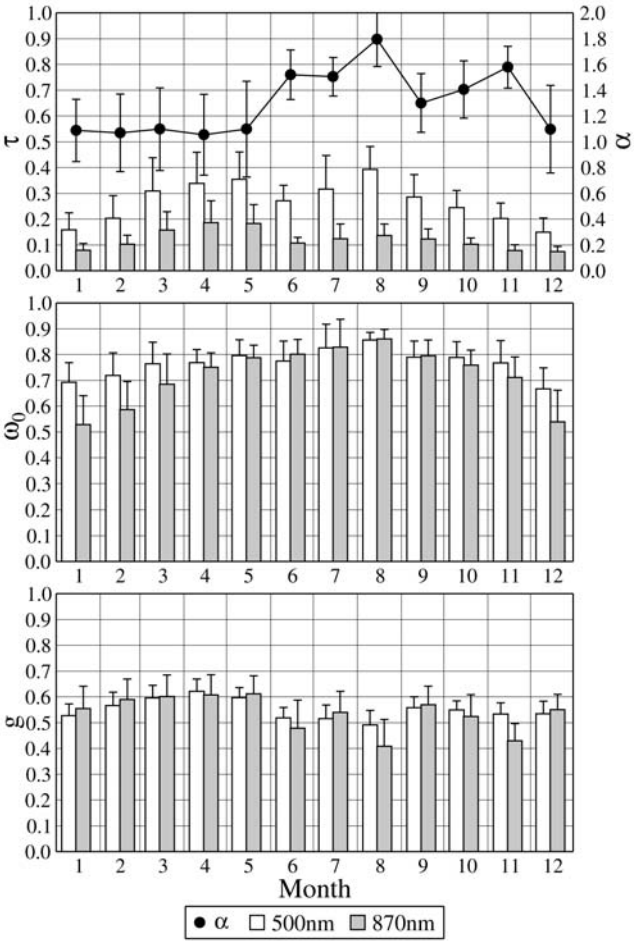

Figure 7. Monthly means of τ, α, ω_0, and g. The vertical error bar indicates the standard deviation from the monthly mean.

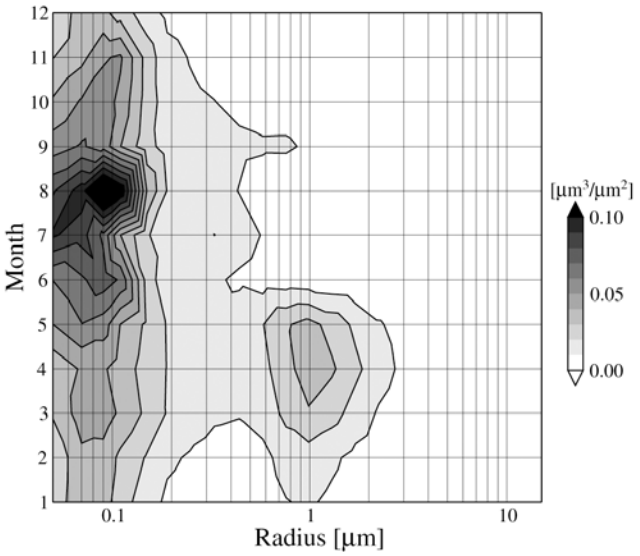

Figure 8. Monthly mean of the volume size distribution.

was from 0.53 to 0.86 and also had the same seasonal variation as $\omega_0(500)$. The difference between $\omega_0(500)$ and $\omega_0(870)$ was large in winter. This is a feature of BC. In general, ω_0 of BC is very small at all wavelengths and also becomes smaller at longer wavelengths. In the winter, local emission of BC might increase as a result of more combustion of fuels than in the other seasons. Furthermore, *Kaneyasu et al.* [2000] suggest that carbon-rich aerosols from the Asian continent pass over Japan in winter.

[21] The monthly means of g are illustrated in Figure 7. Variable $g(500)$ was from 0.49 to 0.62, and $g(870)$ was from 0.41 to 0.61. They were large in spring and small in summer. Variable g is determined by the size distribution. It is large when the coarse particles are dominant. In spring, dust particles are transported from the Asian continent and the coarse particles become more dominant than in the other seasons. However, it must be noted that there is a possibility of underestimating g because of the uncertainty in the size distribution at radius >1 μm.

3.3. Aerosol Surface Net Radiative Forcing

[22] Figure 9 shows AF^{24} and AFE^{24}. AF^{24} (*TTL*) was from -8.3 to -22.8 W/m^2, large in spring to summer and small in winter. These values were almost the same as the works of *Takayabu et al.* [1999]. AF^{24} (*VIS*) was from -4.9 to -18.1 W/m^2, large from March to June and small from July to August and in winter. AF^{24} (*NIR*) was from -3.3 to -9.1 W/m^2, large from spring to summer and small in winter. These seasonal changes of AF^{24} (*TTL*), AF^{24} (*VIS*), and AF^{24} (*NIR*) were almost consistent with those of $\tau(500)$ and $\tau(870)$. However, AF^{24} (*VIS*) in summer was not consistent with $\tau(500)$. Variable $\tau(500)$ was small in June and large from July to August, but AF^{24} (*VIS*) was large in June and small from July to August.

[23] The monthly means of AFE^{24} are shown in Figure 9. The seasonal change of AFE^{24} (*TTL*) was from -38.4 to -80.0 W/m^2, largest in June and small from July to August. AFE^{24} (*VIS*) was from -17.3 to -60.8 W/m^2, largest in June and small from July to August. AFE^{24} (*NIR*) was from -39.8 to -62.5 W/m^2, large from summer to winter and small in spring. The disagreement between AF^{24} (*VIS*) and $\tau(500)$ in summer was caused by large AFE^{24} (*VIS*) in June and small AFE^{24} (*VIS*) from July to August. In general, AFE^{24} is large when ω_0 is small. However, the seasonal changes of AFE^{24} (*TTL*), AFE^{24} (*VIS*), and AFE^{24} (*NIR*) were not consistent with those of $\omega_0(500)$ and $\omega_0(870)$. We investigate the dependencies of AF^{24} and AFE^{24} on τ, ω_0, and g in the next section.

3.4. Relationship Between Aerosol Optical Properties and Surface Net Radiative Forcing

[24] In this section, we consider how AF^{24} depends on optical properties. According to *Nakajima et al.* [2003], AF^{24} is described by a single-scattering and two-stream approximation as

$$AF^{24} = -(1 - Rs)[1 - \omega_0(1 + g)/2]\tau\left(T_u S_0 D/R^2\right), . \qquad (7)$$

where T_u is the transmittance of the atmosphere except for aerosols, D is the daytime fraction, R is the Earth-to-Sun

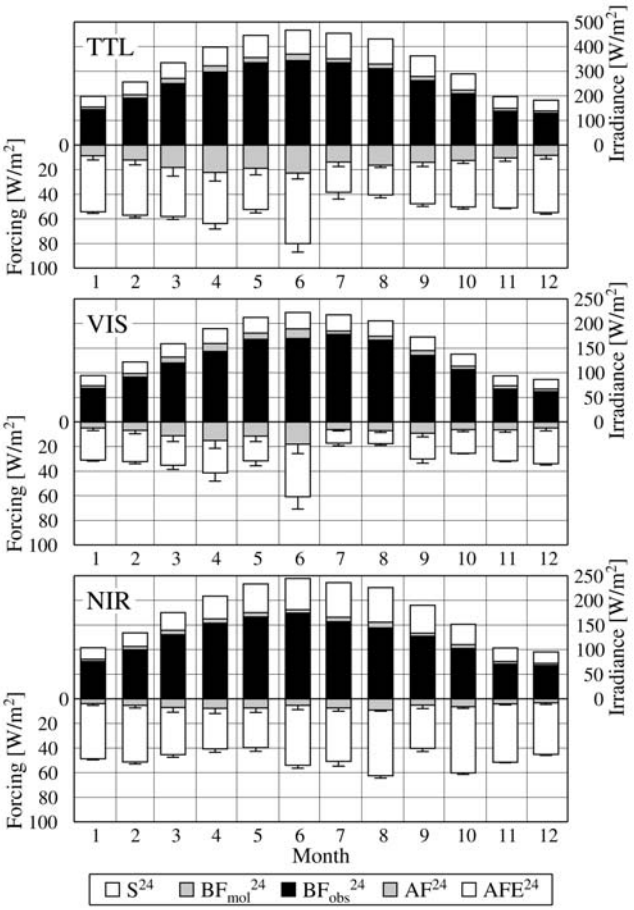

Figure 9. Monthly means of the daily means of the solar irradiance at the top of the atmosphere (S^{24}), the global irradiance calculated without aerosols (BF^{24}_{mol}), the measured global irradiance (BF^{24}_{obs}), the net surface radiative forcing (AF^{24}), and the net surface radiative forcing efficiency (AFE^{24}). S^{24}, BF^{24}_{mol}, and BF^{24}_{obs} are positive values; AF^{24} and AFE^{24} are negative values.

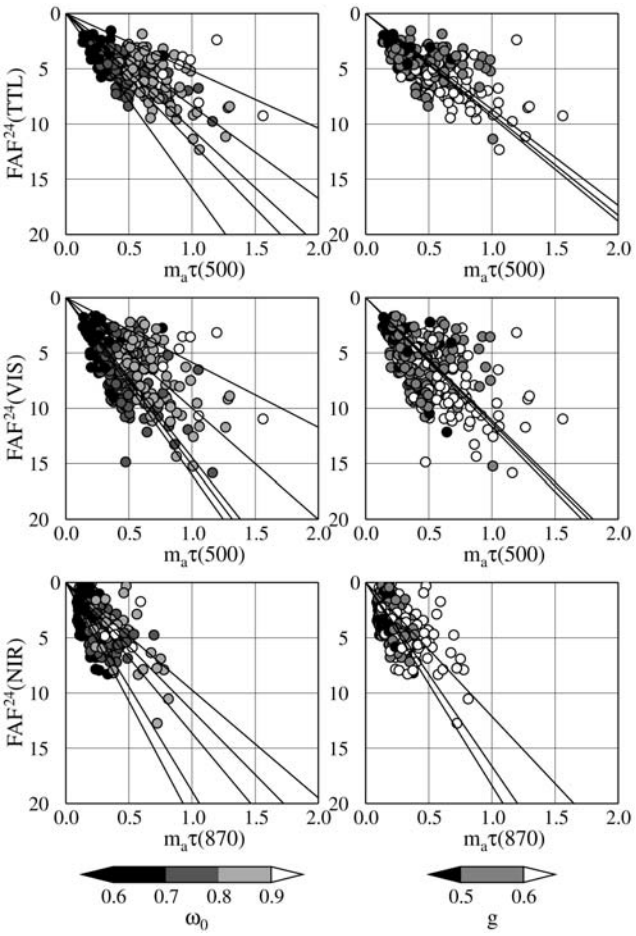

Figure 10. Dependencies of FAF^{24} and $FAFE^{24}$ on $m_a\tau$, ω_0, and g. Shading indicates (left) ω_0 and (right) g. Solid lines in each plot on the left are $FAFE^{24}$ for (top to bottom) $\omega_0 \geq 0.9$, $0.8 \leq \omega_0 < 0.9$, $0.7 \leq \omega_0 < 0.8$, $0.6 \leq \omega_0 < 0.7$, and $\omega_0 < 0.6$. Solid lines in each plot on the right are $FAFE^{24}$ for (top to bottom) $g \geq 0.6$, $0.5 \leq g < 0.6$, and $g < 0.5$.

distance in astronomical units, and S_0 is the solar constant. AF^{24} is influenced by parameters other than aerosol parameters. In particular, the seasonal change of the daily mean solar irradiance at the top of the atmosphere S^{24} is very large (Figure 9). This may affect the seasonal variations of AF^{24} and AFE^{24}. Therefore, we define the fractional forcing FAF^{24} as the percentage of AF^{24} to S^{24}. FAF^{24} is described by

$$S^{24} = S_0 D/\left(m_a R^2\right), \tag{8}$$

$$FAF^{24} = \frac{AF^{24}}{S^{24}} = -(1 - Rs)[1 - \omega_0(1 + g)/2]T_u m_a \tau, \tag{9}$$

where m_a is the daily mean of optical air mass. FAF^{24} was first introduced by *Bush and Valero* [2003]. FAF^{24} cannot be influenced by the seasonal and spatial differences of the solar irradiances. We also defined the fractional radiative forcing efficiency $FAFE^{24}$ as FAF^{24} per unit $m_a\tau$.

[25] The dependencies of FAF^{24} and $FAFE^{24}$ on $m_a\tau$, ω_0, and g were investigated. Figure 10 shows FAF^{24} and $FAFE^{24}$ as functions of $m_a\tau$, ω_0, and g. FAF^{24} was almost proportional to $m_a\tau$. $FAFE^{24}$ decreased with increasing ω_0 and g. $FAFE^{24}$ (*TTL*) and $FAFE^{24}$ (*VIS*) depended only on ω_0 (500). However, $FAFE^{24}$ (*NIR*) depended on both ω_0 (870) and g(870). The magnitude of g(870) is influenced by the existence of coarse particles. The dependence of $FAFE^{24}$ (*NIR*) on g(870) is considered to be a result of the large seasonal change of the coarse particles.

[26] Figure 11 depicts the monthly means of FAF^{24} and $FAFE^{24}$. The seasonal change of FAF^{24} (*TTL*) was from −3.1% to −5.6%, large in spring and small in summer. FAF^{24} (*VIS*) was from −2.8 to −8.1%, large from March to June and small from July to August. FAF^{24} (*NIR*) was from −2.2 to −4.1%. The variation of FAF^{24} (*NIR*) was very small, and the seasonal characteristics was not clear. Compared with the seasonal changes of AF^{24} in Figure 9, FAF^{24} becomes smaller in summer and larger in winter. This means that the magnitude of AF^{24} in winter is smaller than that in summer, but the aerosols in winter reduce the solar irradiance more effectively than in summer.

[27] Figure 11 also presents the monthly mean of $FAFE^{24}$. $FAFE^{24}$ (*TTL*) was from −4.4 to −15.5%, large in winter and small in summer. $FAFE^{24}$ (*VIS*) was from −4.1 to

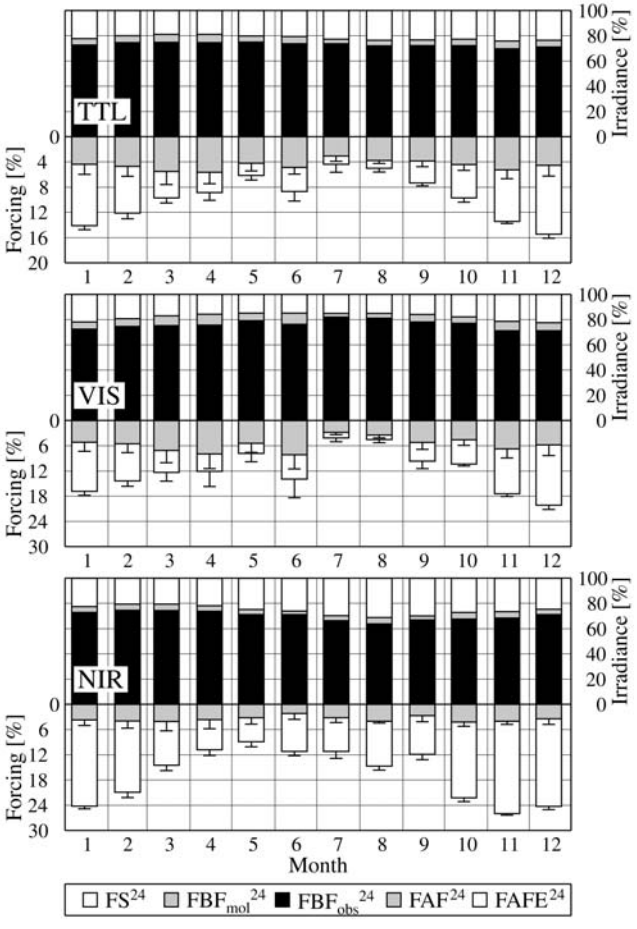

Figure 11. Same as Figure 9, but FS^{24}, FBF^{24}_{mol}, FBF^{24}_{obs}, FAF^{24}, and $FAFE^{24}$ are percentages of S^{24}, BF^{24}_{mol}, BF^{24}_{obs}, AF^{24}, and AFE^{24} to S^{24}.

Table 1. Aerosol Optical Properties and Surface Net Radiative Forcing in East Asia and Optical Properties of Typical Aerosols in the World

Country	Location	τ, Wavelength (nm)	ω_0, Wavelength (nm)	g, Wavelength (nm)	AF^{24} (*TTL*) (W/m^2)	AFE^{24} (*TTL*) (W/m^2)	Reference
Asian continent							
Mongolia	Mandalgovi (45.59°N, 106.19°E)	0.1–1.3[a], 500	0.92–0.95, 500				*Kim et al.* [2004]
China	Inner Mongolia (42.68°N, 115.95°E)	0.2–0.4[a], 670					*Cheng et al.* [2006]
	Lianing (41.51°N, 122.70°E)	0.5–0.6[a], 670					*Cheng et al.* [2006]
	Dunhuang (40.16°N, 94.80°E)	0.1–0.8[a], 500	0.90–0.91, 500				*Kim et al.* [2004]
			0.89, 500	0.71, 500		−76	*Kim et al.* [2005]
		0.3–1.0[a], 670					*Cheng et al.* [2006]
	Beijing (39.98°N, 116.38°E)	0.50–1.25, 440	0.87–0.92, 440	0.65–0.72, 440	−17.2 to −63.5	−65 to −85[a]	*Xia et al.* [2007a]
		0.3–1.1[a], 670					*Cheng et al.* [2006]
	Xianghe (39.75°N, 116.96°E)	0.2–0.6[a], 670			−14.3 to −48.8	−39.9 to −70.2	*Cheng et al.* [2006] *Xia et al.* [2007b]
	Yinchuan (38.48°N, 106.22°E)	0.1–1.0[a], 500	0.90–0.92, 500				*Kim et al.* [2004]
			0.90, 500	0.67, 500		−55	*Kim et al.* [2005]
	Yulin (38.28°N, 109.72°E)	0.1–0.4[a], 670					*Cheng et al.* [2006]
	Taihu (31.70°N, 120.36°E)	0.60–0.90, 500	0.87–0.94, 440	0.71–0.73, 440	−20 to −64[a]	−42 to −64	*Xia et al.* [2007c]
Thailand	Sri-Samrong (17.17°N, 99.87°E)	0.1–1.2[a], 500	0.87–0.94, 500				*Kim et al.* [2004]
			0.88, 500	0.62, 500		−63	*Kim et al.* [2005]
Japan	Sapporo (43.08°N, 141.34°E)	0.21–0.38, 500					*Aoki and Fujiyoshi* [2003]
			0.65, 632.8, winter				*Hayasaka et al.* [1992]
	Sendai (38.25°N, 140.84°E)		0.69–0.93, 632.8				*Hayasaka et al.* [1992]
	Niigata (37.92°N, 139.00°E)	0.26–0.44, 500					*Aoki and Fujiyoshi* [2003]
	Tsukuba (36.05°N, 140.13°E)	0.15–0.39, 500	0.67–0.86, 500	0.49–0.62, 500	−8.3 to −22.8	−38.4 to −80.0	this study
			0.69–0.87, 500				*Nishizawa et al.* [2004]
		0.18–0.37, 500					*Aoki and Fujiyoshi* [2003]
					−7.8 to −35.1		*Takayabu et al.* [1999]
	Tokyo (35.66°N, 139.80°E)	0.20–0.45, 500					*Aoki and Fujiyoshi* [2003]
Typical aerosols							
Urban-industrial and mixed		0.24–0.43, 440	0.90–0.98, 440	0.68–0.74, 440			*Dubovik et al.* [2002]
Biomass burning		0.38–0.80, 440	0.88–0.94, 440	0.64–0.69, 440			*Dubovik et al.* [2002]
Desert dust and oceanic		0.04–0.39, 440	0.92–0.98, 440	0.68–0.75, 440			*Dubovik et al.* [2002]

[a]Values were read from the figures in the references.

−20.1% and exhibited the same seasonal change as $FAFE^{24}$ (*TTL*). $FAFE^{24}$ (*NIR*) was from −8.9 to −26.0%, large in winter and small in spring. The seasonal changes of $FAFE^{24}$ correspond to those of ω_0. Furthermore, large $FAFE^{24}$ (*NIR*) in summer and small $FAFE^{24}$ (*NIR*) in spring were consistent with small $g(870)$ in summer and large $g(870)$ in spring. The fractional radiative forcing excluded the solar seasonal effect and clarified the aerosol radiative effect.

3.5. Comparison With Other Sites Over East Asia

[28] East Asia is one of the world's major aerosol sources. The aerosols spread from the Asian continent to the North Pacific Ocean via Japan by the westerlies in the midlatitudes. The atmosphere over Japan is influenced by the continental aerosols. We compared the seasonal characteristics of the aerosol optical properties and surface net radiative forcing in Japan to those in the Asian continent. The optical properties of the continental aerosols are estimated from the measurements of the solar direct and sky radiances at SKYNET and AERONET sites. Table 1 lists the optical properties and surface net radiative forcing at the surface in Japan and the Asian continent. We collected the results of the seasonal changes in the references. Moreover, the optical properties of the typical aerosols were also given in Table 1. They were obtained from the measurements at various sites of AERONET in the world [*Dubovik et al.*, 2002].

[29] Variable τ of the continental aerosols was from 0.1 to 1.3 and large in spring to summer. The annual mean was about 0.5. High τ was mostly attributed to dust events in spring and pollutant particles in summer. The seasonal change of τ in Japan was almost the same as that over the continent. However, τ in Japan was small, from 0.15 to 0.44. The annual mean was about 0.3.

[30] Variables ω_0 and g are important parameters for determining the aerosols' radiative effect. Variable ω_0 of the continental aerosols was from 0.87 to 0.95 and was large in summer. The annual mean was about 0.9 and comparable to the typical aerosols. Variable ω_0 in Tsukuba was from 0.67 to 0.87, and the seasonal change was the same as for the continental aerosols. In spite of the importance of ω_0 and g, very little is currently available in the published literature on the seasonal characteristics of ω_0 and g in Japan. *Hayasaka et al.* [1992] have published the seasonal change of ω_0 by in situ sampling measurements. Their result was from 0.65 to 0.93, large in summer and small in winter. Variable ω_0 in Japan had the same seasonal change as the continental aerosols but was smaller than the continental aerosol, particularly in winter. BC is a greatest contributor to the decrease in ω_0. The fraction of BC in Japan may be larger than that over the continent. Some studies by in situ sampling measurements showed high fraction of BC at urban sites in Japan [*Hasegawa and Ohta*, 2002; *Höller et al.*, 2002]. Furthermore, *Zhang et al.* [2008] demonstrate that the ratios of organic carbon (OC) to elemental carbon (EC) in China are higher than at other locations in East Asia, from the analysis of OC and EC concentrations measured at 18 stations of the China Atmosphere Watch Network. EC is frequently called BC. High OC/EC ratio implies that ω_0 in China is higher than that at other sites in East Asia, because OC is less absorptive than EC. However, ω_0 depends on not only a fraction of BC but also the mixing state of BC and the optical properties of the other aerosols than BC. In order to explain small ω_0 in Japan, we need further studies of the radiation measurements together with the chemical analysis.

[31] Variable g of the continental aerosols was from 0.62 to 0.73 and was comparable to the typical aerosols. However, g at Tsukuba was small, from 0.49 to 0.62. There is a possibility of underestimating g at Tsukuba because of the uncertainty in the estimated size distribution, but the bias error is about 0.06 [*Kudo et al.*, 2008]. Variable g at Tsukuba is smaller than the continental aerosols. The characteristic of the size distribution in the Asian continent was dominant coarse particles throughout a year because of the desert regions on the continent [*Kim et al.*, 2004; *Cheng et al.*, 2006]. By contrast, the coarse particles in Tsukuba were not dominant except in spring. Furthermore, *Uchiyama et al.* [2005a] found that the coarse particles during the spring dust event are partially removed during the transport to Japan. Therefore, g at Tsukuba would be smaller than that over the continent throughout a year.

[32] AF^{24} (TTL) of the continental aerosols was from -14 to -64 W/m^2 and was large in spring to summer. In Japan, AF^{24} (TTL) is from -8.3 to -22.8 W/m^2 and is large in spring to summer. The small AF^{24} (TTL) in Japan is attributed to small τ.

[33] Variables ω_0 and g in Japan were quite different from those in the continent, but AFE^{24} in Japan, from -38.4 to -80.0 W/m^2, was comparable to that in the continent, from -40 to -85 W/m^2. AFE^{24} cannot be determined by ω_0 and g alone. The fractional radiative forcing efficiency excludes the spatial and seasonal differences of the solar irradiance, and the aerosol radiative effects at the different sites would become clear.

4. Summary

[34] We have observed the direct and diffuse irradiances in the VIS and NIR regions by two spectral and four broadband radiometers from April 2004 to March 2008. Using these measurements under cloudless conditions, the seasonal characteristics of the aerosol optical properties and surface net radiative forcing in Tsukuba were evaluated. The following clear seasonal characteristics were obtained. Variable τ was from 0.15 to 0.39 at 500 nm and from 0.07 to 0.19 at 870 nm. Variable τ, at both 500 and 870 nm, was large in spring and summer and small in winter. From the seasonal changes of α and the size distribution, the coarse particles were dominant in spring and the small particles were dominant in summer. Variable ω_0 was from 0.67 to 0.86 at 500 nm and from 0.53 to 0.86 at 870 nm. Variable ω_0, at both 500 and 870 nm, was large in summer and small in winter. The difference between 500 and 870 nm was large in winter. It can be deduced that the fraction of BC in aerosols become large in winter. Variable g was from 0.49 to 0.62 at 500 nm and from 0.41 to 0.61 at 870 nm. This g, at both 500 and 870 nm, was large in spring and small in summer. Large g in spring is due to the transported dust particles from the Asian continent. However, it must be noted that there is a possibility of underestimating g because of the uncertainty in the size distribution. AF^{24} was from -8.3 to -22.8, -4.9 to -18.1, and -3.3 to -9.1 W/m^2 in the TTL, VIS, and NIR regions, respectively. AF^{24} in the TTL, VIS, and NIR regions was large in summer and small in winter. The seasonal changes of AF^{24} were almost consistent with those of τ. AFE^{24} was from -38.4 to -80.0, -17.3 to -60.8, and -39.8 to -62.5 W/m^2 in the TTL, VIS, and NIR regions, respectively. The seasonal changes of AFE^{24} was not consistent with those of ω_0 and g. However, the seasonal changes of $FAFE^{24}$, which is defined as the ratio of AFE^{24} to the solar irradiance at the top of the atmosphere, were consistent with those of ω_0 in the TTL, VIS, and NIR regions. Furthermore, the dependency of $FAFE^{24}$ on g was seen in NIR region. The seasonal changes of aerosol radiative effects were clarified by $FAFE^{24}$.

[35] The aerosols in the Asian continent are frequently transported to the North Pacific Ocean via Japan by the westerlies in the mid-latitudes. We compared the seasonal characteristics of τ, ω_0, g, AF^{24}, and AFE^{24} to those at other sites in East Asia from the view point of the differences between Japan and the Asian continent. The annual mean of τ in Japan was about 0.3 and that over the continent was about 0.5. Variable ω_0 in Japan was from 0.65 to 0.93, and that over the continent was from 0.87 to 0.95. It may be deduced that a fraction of BC in Japan is larger than that over the continent. Variable g in Japan was from 0.49 to 0.62, and that over the continent was from 0.62 to 0.73. This is due to the fact that coarse particles are dominant over the continent at all seasons but not in Japan. AF^{24} in Japan was

from −8.3 to −22.8 W/m^2, and that over the continent was from −14 to −64 W/m^2. The difference of AF^{24} would be due to the difference of τ. AFE^{24} in Japan was almost the same as that over the continent in spite of the differences of ω_0 and g. We should use $FAFE^{24}$ for comparing the radiative effects of ω_0 and g at different sites.

[36] The aerosol optical properties and surface net radiative forcing in Japan were very different from those in the Asian continent. The results suggest that the aerosol components in Japan are different from in the Asian continent. As a future study, the continuous and simultaneous measurements of the solar radiation and the aerosol chemical properties are necessary to explain the differences of the aerosol optical properties and radiative forcing between Japan and the Asian continent.

References

Aoki, K., and Y. Fujiyoshi (2003), Sky radiometer measurements of aerosol optical properties over Sapporo, Japan, *J. Meteorol. Soc. Jpn.*, *81*, 493–513.

Asano, S., and M. Shiobara (1989), Aircraft measurements of the radiative effects of tropospheric aerosols: 1. Observational results of the radiation budget, *J. Meteorol. Soc. Jpn.*, *67*, 847–861.

Asano, S., et al. (1997), A sonde system for simultaneous measurements of radiative fluxes and cirrus microphysics in the Japanese Cloud-Climate Study (JACCS) program, in *IRS'96: Current Problems in Atmospheric Radiation*, edited by W. L. Smith and K. Stamnes, pp. 349–352, A. Deepak, Hampton, Va.

Bush, B. C., and F. P. J. Valero (2003), Surface aerosol radiative forcing at Gosan during the ACE-Asia campaign, *J. Geophys. Res.*, *108*(D23), 8660, doi:10.1029/2002JD003233.

Charlson, R. J., S. E. Schwartz, J. M. Hales, D. Cess, J. A. Coakley, and J. E. Hansen (1992), Climate forcing by anthropogenic aerosols, *Science*, *255*, 423–430.

Cheng, T., H. Wang, Y. Xu, H. Li, and L. Tian (2006), Climatology of aerosol optical properties in northern China, *Atmos. Environ.*, *40*, 1495–1509.

Chou, M. D., and W. Zhao (1997), Estimation and model validation of surface radiation and cloud radiative forcing using TOGA COARE measurements, *J. Clim.*, *10*, 610–620.

Cornette, W. M., and J. G. Shanks (1992), Physically reasonable analytic expression for the single-scattering phase function, *Appl. Opt.*, *31*, 3152–3160.

Dubovik, O., B. Holben, T. F. Eck, A. Smirnov, Y. J. Kaufman, M. D. King, D. Tanre, and I. Slutsker (2002), Variability of absorption and optical properties of key aerosol types observed in worldwide locations, *J. Atmos. Sci.*, *59*, 590–608.

Hasegawa, S., and S. Ohta (2002), Some measurements of the mixing state of soot-containing particles at urban and non-urban sites, *Atmos. Environ.*, *36*, 3899–3908.

Hayasaka, T., T. Nakajima, S. Ohta, and M. Tanaka (1992), Optical and chemical properties of urban aerosols in Sendai and Sapporo, Japan, *Atmos. Environ.*, *26*, 2055–2062.

Hayasaka, T., Y. Sasano, and T. Takamura (1998), Stratification and size distribution of aerosols retrieved from simultaneous measurements with Lidar, a sunphotometer, and an aureolemeter, *Appl. Opt.*, *37*, 961–970.

Holben, B. N., et al. (1998), AERONET-A federated instrument network and data archive for aerosol characterization, *Remote Sens. Environ.*, *66*, 1–16.

Höller, R., S. Tohno, M. Kasahara, and R. Hitzenberger (2002), Long-term characterization of carbonaceous aerosol in Uji, Japan, *Atmos. Environ.*, *36*, 1267–1275.

Kaneyasu, N., K. Takeuchi, M. Hayashi, S. Fujita, I. Uno, and H. Sasaki (2000), Outflow patterns of pollutants from East Asia to the North Pacific in the winter monsoon, *J. Geophys. Res.*, *105*, 17,361–17,377.

Kasten, F., and T. Young (1989), Revised optical air mass tables and approximation formula, *Appl. Opt.*, *28*, 4735–4738.

Kim, D., B. J. Sohn, T. Nakajima, T. Takamura, T. Takemura, B. C. Choi, and S. C. Yoon (2004), Aerosol optical properties over East Asia determined from ground-based sky radiation measurements, *J. Geophys. Res.*, *109*, D02209, doi:10.1029/2003JD003387.

Kim, D., B. J. Sohn, T. Nakajima, and T. Takamura (2005), Aerosol radiative forcing over East Asia determined from ground-based solar radiation measurements, *J. Geophys. Res.*, *110*, D10S22, doi:10.1029/2004JD004678.

Kudo, R., A. Uchiyama, A. Yamazaki, E. Kobayashi, and T. Nishizawa (2008), Retrieval of aerosol single-scattering properties from diffuse and direct irradiances: Numerical studies, *J. Geophys. Res.*, *113*, D09204, doi:10.1029/2007JD009239.

Lacis, A. A., and J. E. Hansen (1974), A parameterization for the absorption of solar radiation in the Earth's atmosphere, *J. Atmos. Sci.*, *31*, 119–133.

Long, C. N., and T. P. Ackerman (2000), Identification of clear skies from broadband pyranometer measurements and calculation of downwelling shortwave cloud effects, *J. Geophys. Res.*, *105*, 15,609–15,626.

López, G., and F. J. Batlles (2004), Estimation of the atmospheric turbidity from three broad-band solar radiation algorithms. A comparative study, *Ann. Geophys.*, *22*, 2657–2668.

Molineaux, B., P. Ineichen, and J. J. Delaunay (1995), Direct luminous efficacy and atmospheric turbidity–improving model performance, *Sol. Energ.*, *55*, 125–137.

Nakajima, T., et al. (2003), Significance of direct and indirect radiative forcings of aerosols in the East China Sea region, *J. Geophys. Res.*, *108*(D23), 8658, doi:10.1029/2002JD003261.

Nishizawa, T., S. Asano, A. Uchiyama, and A. Yamazaki (2004), Seasonal variation of aerosol direct radiative forcing and optical properties estimated from ground-based solar radiation measurements, *J. Atmos. Sci.*, *61*, 57–72.

Pradeep, K., and Y. Ishizaka (2007), Effects of continentally polluted air mass on aerosol optical properties over the East China Sea, *J. Meteorol. Soc. Jpn.*, *85*, 47–68.

Perez, R., P. Ineichen, R. Seals, and A. Zelenka (1990), Making full use of the clearness index for parameterizing hourly insolation conditions, *Sol. Energ.*, *45*, 111–114.

Schmid, B., K. J. Thome, P. Demoulin, R. Peter, C. Mätzler, and J. Sekler (1996), Comparison of modeled and empirical approaches for retrieving columnar water vapor from solar transmittance measurements in the 0.94-μm region, *J. Geophys. Res.*, *101*, 9345–9358.

Takayabu, Y. N., T. Ueno, T. Nakajima, I. Matsui, Y. Tsushima, K. Aoki, N. Sugimoto, and I. Uno (1999), Estimate of the cloud and aerosol effects on the surface radiative flux based in the measurements and the transfer model calculations part: Shortwave forcing at Tateno, Japan, *J. Meteorol. Soc. Jpn.*, *77*, 1007–1021.

Uchiyama, A., A. Yamazaki, H. Togawa, and J. Asano (2005a), Characteristics of aeolian dust observed by sky-radiometer in the intensive observation period 1 (IOP1), *J. Meteorol. Soc. Jpn.*, *83A*, 291–305.

Uchiyama, A., A. Yamazaki, H. Togawa, J. Asano, and G. Shi (2005b), Single scattering albedo of aeolian dust as inferred from sky-radiometer and in situ ground-based measurement, *SOLA*, *1*, 209–212.

Waliser, D. E., W. D. Collins, and S. P. Anderson (1996), An estimate of the surface shortwave cloud forcing over the western pacific during TOGA COARE, *Geophys. Res. Lett.*, *23*, 519–522.

Won, J. G., S. C. Yoon, S. W. Kim, A. Jefferson, E. G. Dutton, and B. N. Holben (2004), Estimation of direct radiative forcing of Asian dust aerosols with Sun/Sky radiometer and Lidar measurements at Gosan, Korea, *J. Meteorol. Soc. Jpn.*, *82*, 115–130.

Xia, X., H. Chen, P. Goloub, W. Zhang, B. Chatenet, and P. Wang (2007a), A complication of aerosol optical properties and calculation of direct radiative forcing over an urban region in northern China, *J. Geophys. Res.*, *112*, D12203, doi:10.1029/2006JD008119.

Xia, X., Z. Li, P. Wang, H. Chen, and M. Cribb (2007b), Estimation of aerosol effects on surface irradiance based on measurements and radiative transfer model simulations in northern China, *J. Geophys. Res.*, *112*, D22S10, doi:10.1029/2006JD008337.

Xia, X., Z. Li, B. Holben, P. Wang, T. Eck, H. Chen, M. Cribb, and Y. Zhao (2007c), Aerosol optical properties and radiative effects in the Yangtze Delta region of China, *J. Geophys. Res.*, *112*, D22S12, doi:10.1029/2007JD008859.

Zhang, X. Y., Y. Q. Wang, X. C. Zhang, W. Guo, and S. L. Gong (2008), Carbonaceous aerosol composition over various regions of China during 2006, *J. Geophys. Res.*, *113*, D14111, doi:10.1029/2007JD009525.

E. Kobayashi, Aerological Observatory, Japan Meteorological Research Agency, 1-2 Nagamine, Tsukuba 305-0052, Japan.

R. Kudo, A. Uchiyama, and A. Yamazaki, Meteorological Research Institute, Japan Meteorological Agency, 1-1 Nagamine, Tsukuba 305-0052, Japan. (reikudo@mri-jma.go.jp)